Systematic behavior of the Mie scattering coefficients of spheres as a function of order

I. K. Ludlow and J. Everitt
Division of Physical Sciences, University of Hertfordshire, College Lane, Hatfield, Hertfordshire AL10 9AB, United Kingdom
(Received 10 October 1995)

The Mie scattering coefficients of large homogeneous dielectric spheres are shown to vary systematically with order. A general analysis of the coefficients gives formulas that depend only on two real electric and magnetic multipole phase angles. Such angles decrease in a quasimonotonic manner with order and explain the cutoff of Mie and Gegenbauer coefficients at order $n \approx \alpha$, the outer size parameter of the sphere, independently of the refractive index to first order. When the relative refractive index of the sphere m is moderately greater than unity, the multipole phase angles become integer values of π at large orders and approach zero by a sequence of steps in the form of a descending staircase. It is also shown that Rayleigh-Debye scattering corresponds to the limiting case of $m-1 \rightarrow 0$.

PACS number(s): 42.25.Fx, 02.30.Qy, 92.60.Mt

I. INTRODUCTION

It is well known that the Mie theory of light scattering offers a rigorous treatment for the calculation of scattering patterns of isotropic homogeneous and layered spheres. This being so, it is hardly surprising that theoreticians have shown little recent interest in the scattering from spheres. A need, nevertheless, still exists for theoretical studies with the aim of establishing an optimal inversion procedure for particle characterization from experimental scattering patterns.

In a standard scattering arrangement, a polarized laser beam is directed onto a particle and the scattered light is collected over a detector array to produce a quasicontinuous distribution of irradiance over scattering angles of nearly 180° in the plane of detection. The problem faced by the experimentalist is then to determine the particle size and refractive index from such data. In the case of homogeneous or coated spheres, this is possible by matching the experimental patterns to those of a theoretical database [1–3]. Unfortunately, the procedure requires large amounts of computer memory and cannot be performed in real time. A question may also be raised concerning the uniqueness of the "best fit" theoretical pattern.

The above inversion technique may be contrasted with that of holography, where the storage of both the amplitude and phase of the scattered field is a necessary requirement for object reconstruction. Since the normal scattering pattern contains no phase information, the success of the pattern matching as a means of inversion must therefore be explained as being due to the restrictions placed on the amplitude scattering functions a_n and b_n of the particle by the requirement of spherical symmetry.

Notwithstanding the value of heuristic methods for particle characterization, techniques should be sought that can be theoretically justified. An essential step in this respect is the derivation of a procedure that relates the scattered electric field to the irradiance pattern. Such a relationship cannot be obtained from the Mie scattering formulas since the angular functions $\tau_n(\cos\vartheta)$ and $\pi_n(\cos\vartheta)$ do not form a complete orthogonal set for scattering angles ϑ in the range 0°–180°. The Mie equations can, however, be reformulated in terms of Gegenbauer functions $T_n^1(\cos\vartheta)$, which do comprise a complete orthogonal set [4]. As a consequence, the scattered field and irradiance in the plane of detection can both be represented by Gegenbauer series. This has a number of advantages.

(a) The angular dependence of a scattering pattern can be eliminated by transforming it into a discrete Gegenbauer spectrum. This is constructed by plotting the Gegenbauer coefficients of the irradiance as a function of the order n. In general, such spectra have a simpler structure than the original data.

(b) The Gegenbauer spectra exhibit a high-order cutoff at $n \approx 2\alpha$ from which particle size may be determined.

(c) A set of equations relating Gegenbauer coefficients of the irradiance to the products of the amplitude Gegenbauer coefficients may be obtained.

The analysis clearly offers opportunities for particle characterization, but practical difficulties need to be considered. Of these, the most important is missing data due to the entrance and exit apertures of the irradiating laser beam or detector saturation for forward scattering. The latter may be prevented by instrumental design, while the former is unavoidable. Nevertheless, the absent data can be recovered by assuming forward and backward scattering to be of the form $A + B\sin^2(\vartheta/2) + C\sin^4(\vartheta/2)$ and comparing the resultant high-order ripple in the spectrum with that obtained from the experimental results.

Features (a) and (b) of the Gegenbauer analysis of scattering patterns could be used as the basis of efficient particle fitting by matching the experimental spectrum to theoretical spectra. But an even more powerful method of analysis appears possible through the use of the equations referred to in (c). Solutions of the equations would yield the amplitude Gegenbauer coefficients from which the scattering field could be reconstructed. Unfortunately, equations of this kind have not been studied previously and methods for their solution need to be investigated. It would therefore be informative to analyze the systematic behavior of the amplitude scattering coefficients a_n and b_n as a function of order. This is the purpose of the present paper.

The analysis will show that the variation of the amplitude coefficients with order can be understood in terms of two

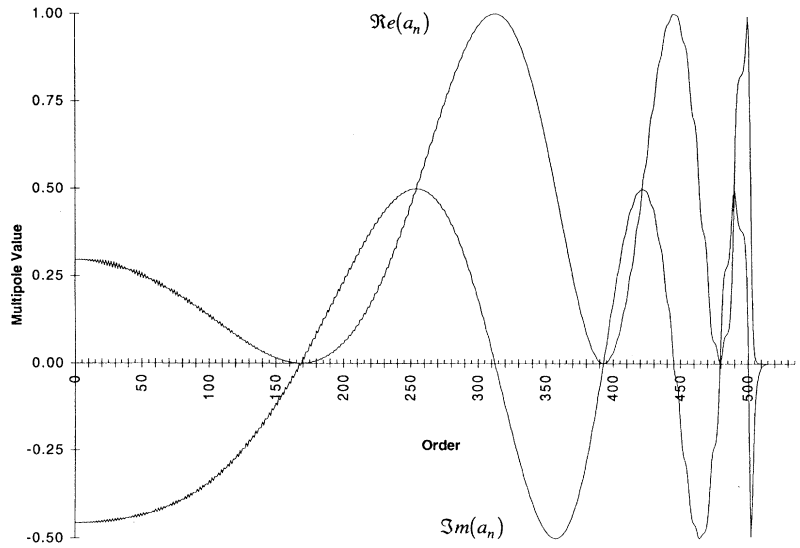

FIG. 1. Variation of $\mathrm{Re}(a_n)$ and $\mathrm{Im}(a_n)$ with order for $\alpha=500.5$, $\beta=510.5$, and $m=1.02$.

multipole phase angles u_n and v_n. Furthermore, absolute values of these phase angles can be defined in terms of amplitude and phase factors of Riccati-Bessel functions of the sphere.

II. MULTIPOLE PHASE ANGLES

We consider a nonabsorbing sphere of radius a with a refractive index m relative to the ambient medium that is irradiated by a collimated monochromatic light beam having a propagation constant k in the ambient medium. The scattering coefficients then depend on just the two factors, the external and internal size parameters of the sphere $\alpha=ka$ and $\beta=m\alpha$.

In the case of perpendicularly polarized scattering, the scattering amplitude has the form [4]

$$S_\perp=\sum_{n=1}^{\infty}\frac{2n+1}{n(n+1)}\{a_n\pi_n(z)+b_n\tau_n(z)\} \tag{1a}$$

$$=\sum_{n=0}^{\infty}(c_n)_\perp T_n^1(z), \tag{1b}$$

where $\pi_n(\cos\vartheta)=P_n^1(\cos\vartheta)/\sin\vartheta$, $\tau_n(\cos\vartheta)=(\partial/\partial\vartheta)P_n^1(\cos\vartheta)$, and $z=\cos\vartheta$ for a scattering angle ϑ. Equation (1a) is Mie's formula with electric and magnetic multipole coefficients a_n and b_n, respectively. This may be reformulated as a Gegenbauer series to give Eq. (1b) in which

$$(c_n)_\perp=\frac{n}{n+1}b_n+\frac{2n+3}{(n+1)(n+2)}a_{n+1}-\frac{n+3}{n+2}b_{n+2}. \tag{2}$$

Equivalent expressions for parallel polarized scattering may be obtained by the interchange $a_s\rightarrow b_s$ and $b_s\rightarrow a_s$.

Electric and magnetic multipole phase angles u_n and v_n can be defined by

$$\tan u_n=\frac{\psi_n'(\beta)\psi_n(\alpha)-m\psi_n(\beta)\psi_n'(\alpha)}{\psi_n'(\beta)\chi_n(\alpha)-m\psi_n(\beta)\chi_n'(\alpha)}, \tag{3a}$$

$$\tan v_n=\frac{m\psi_n'(\beta)\psi_n(\alpha)-\psi_n(\beta)\psi_n'(\alpha)}{m\psi_n'(\beta)\chi_n(\alpha)-\psi_n(\beta)\chi_n'(\alpha)}, \tag{3b}$$

where $\psi_n(\alpha)$ and $\chi_n(\alpha)$ are Riccati-Bessel functions (defined in Appendix A) and yield the scattering coefficients through the relations

$$a_n=\tfrac{1}{2}(1-e^{i2u_n})=-ie^{iu_n}\sin u_n, \tag{4a}$$

$$b_n=\tfrac{1}{2}(1-e^{i2v_n})=-ie^{iv_n}\sin v_n. \tag{4b}$$

As the particle is nonabsorbing, the internal size parameter is real and so are u_n and v_n. The real and imaginary parts of the coefficients are

$$\mathrm{Re}(a_n)=\sin^2 u_n, \tag{5a}$$

$$\mathrm{Im}(a_n)=-\cos u_n\sin u_n, \tag{5b}$$

with similar expressions for b_n.

A few earlier studies concerning the multipole coefficients have been carried out on approximate expressions at low orders and the circular relation between real and imaginary components for varying particle size at a fixed refractive index and order [5]. Our interest, however, is the variation of a_n and b_n with order for a particle having a fixed refractive index and size. Plots of the real and imaginary parts of a_n and b_n are accordingly presented in Figs. 1 and 2 for a particle with $\alpha=500.5$, $\beta=510.5$, and $m=1.02$. Large values were chosen for α and β so as to generate quasicontinuous graphs and $\beta-\alpha=10$ ensures that $m\geqslant 1$.

The principle feature of both figures is an oscillation in n that increases in periodicity with order up to a cutoff value between α and β. Such behavior can be associated with $u_n=v_n$ in which the phase angles decrease monotonically to zero with increasing order. This may be shown by starting

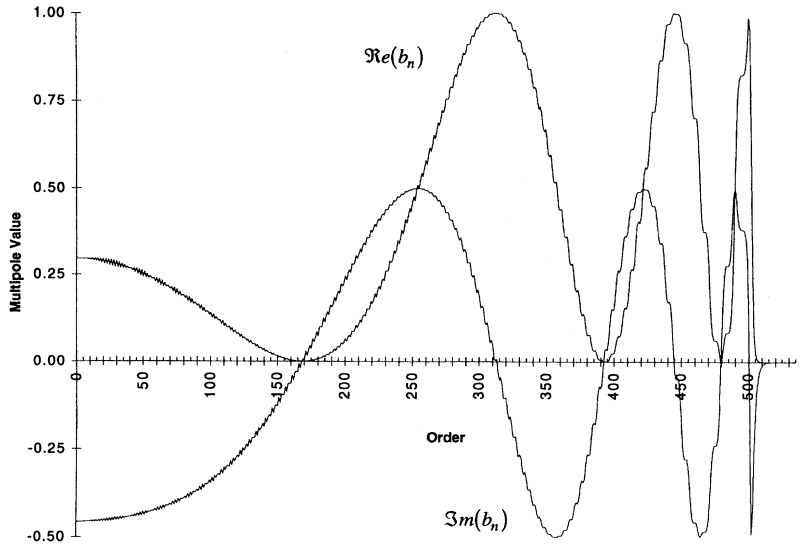

FIG. 2. Variation of $\mathrm{Re}(b_n)$ and $\mathrm{Im}(b_n)$ with order for $\alpha=500.5$, $\beta=510.5$, and $m=1.02$.

from the cutoff order and evaluating the phase angles at the lower orders by interpolating between the values given in Table I obtained from Eqs. (5). Thus the phase angles at zero order are $u_0=v_0\approx 10$ rad. It is no coincidence that $u_0=v_0\approx\beta-\alpha$, as will be shown below.

A second weaker structure of high periodicity is also present in the two figures. This is most noticeable for b_n in which the amplitude of the secondary oscillation increases with order while its periodicity decreases. For the a_n plots, the secondary amplitude initially decreases between $n=0$ and $n\approx 350$ before increasing as the cutoff is approached. Over the complete range, the periodicity reduces with increasing order.

A. Zeroth-order phase angle

Although a_0 and b_0 are not required in calculating light scattering patterns, their phase angles may be readily derived and give a valuable insight into the origin of the structures of Figs. 1 and 2. Using $\psi_0(z)=\sin z$ and $\chi_0(z)=-\cos z$, substitution into Eqs. (3) yields

$$\tan u_0=\frac{m\,\tan\beta-\tan\alpha}{1+m\,\tan\beta\,\tan\alpha}, \tag{6a}$$

$$\tan v_0=\frac{(1/m)\,\tan\beta-\tan\alpha}{1+(1/m)\tan\beta\,\tan\alpha}, \tag{6b}$$

TABLE I. Special values of the phase angles and scattering coefficients. p has integer values.

$\begin{Bmatrix} u_n \\ v_n \end{Bmatrix}$	$\mathrm{Re}\begin{Bmatrix} a_n \\ b_n \end{Bmatrix}$	$\mathrm{Im}\begin{Bmatrix} a_n \\ b_n \end{Bmatrix}$
$p\pi$	0	0
$(p+\frac{1}{4})\pi$	$\frac{1}{2}$	$-\frac{1}{2}$
$(p+\frac{1}{2})\pi$	1	0
$(p+\frac{3}{4})\pi$	$\frac{1}{2}$	$\frac{1}{2}$

These equations may be converted using the identity

$$\tan(A-B)=\frac{\tan A-\tan B}{1+\tan A\,\tan B}.$$

Thus, for Eq. (6a), $u_0=A-B, B=\alpha$, and $A=B+\epsilon$ when

$$m\,\tan\beta=\tan(\beta+\epsilon)=\frac{\tan\beta-\tan\epsilon}{1+\tan\beta\,\tan\epsilon},$$

giving

$$\tan\epsilon=\frac{(m-1)\tan\beta}{1+m\,\tan^2\beta}.$$

This shows that ϵ is an incremental change of β when $\tan\beta$ is multiplied by m. The solution of the phase angle u_0 is therefore

$$u_0=\beta-\alpha+\epsilon=\beta-\alpha+\tan^{-1}\left\{\frac{(m-1)\tan\beta}{1+m\,\tan^2\beta}\right\}, \tag{7a}$$

where the principle component of ϵ is used. Similarly,

$$v_0=\beta-\alpha-\tan^{-1}\left\{\frac{(m-1)\tan\beta}{m+\tan^2\beta}\right\}. \tag{7b}$$

A phase $p\pi$, where p is an arbitrary integer, could in general be added to u_0 and v_0, but to obtain expressions consistent with the definitions and values of the phase angles determined from Figs. 1 and 2 requires $p=0$. We note that the increments are zero when β is an integer value of $\pi/2$ and have maximum amplitudes of $\tan^{-1}\{(m-1)/(2\sqrt{m})\}$ when $\tan\beta=\pm 1/\sqrt{m}$ for u_0 and $\tan\beta=\pm\sqrt{m}$ for v_0.

B. Low-order phase angles

A comparison between explicit expressions of the Riccati-Bessel functions shows that when only the first two leading terms are significant [6],

$$\psi_n(z)=\sin\left(z-\frac{n\pi}{2}\right)+\frac{n(n+1)}{2z}\cos\left(z-\frac{n\pi}{2}\right)+O\left(\frac{n^4}{z^2}\right),$$

$$\chi_n=-\cos\left(z-\frac{n\pi}{2}\right)+\frac{n(n+1)}{2z}\sin\left(z-\frac{n\pi}{2}\right)+O\left(\frac{n^4}{z^2}\right).$$

These expressions may be simplified into

$$\psi_n(z)\approx\psi_0(z'), \tag{8a}$$

$$\chi_n(z)\approx\chi_0(z'), \tag{8b}$$

for which $z'=z-n\pi/2+n(n+1)/(2z)$ when $n^2\ll z$.

An analysis as in Sec. II A then leads to the separation of the phase angles into the dominant and incremental components

$$u_n=\bar{u}_n+\tilde{u}_n, \tag{9a}$$

$$v_n=\bar{v}_n+\tilde{v}_n. \tag{9b}$$

The dominant terms are equal so that

$$\bar{u}_n=\bar{v}_n=\beta'-\alpha'=(\beta-\alpha)\left\{1-\frac{n(n+1)}{2\alpha\beta}\right\}, \tag{10a}$$

whereas the increments are

$$\tilde{u}_n=\tan^{-1}\left\{\frac{(m-1)\tan\beta'}{1+m\tan^2\beta'}\right\} \tag{10b}$$

and

$$\tilde{v}_n=-\tan^{-1}\left\{\frac{(m-1)\tan\beta'}{m+\tan^2\beta'}\right\}. \tag{10c}$$

Such formulas are only valid with $n^2\ll\alpha,\beta$.

Thus the dominant component exhibits a slow variation that decreases monotonically with increasing order while the increments alternate in sign and have a maximum possible amplitude of $\tan^{-1}\{(m-1)/(2\sqrt{m})\}$. We may now identify the principle and secondary structure of Figs. 1 and 2 with the dominant and incremental components, respectively, of the phase angles.

III. GENERAL SOLUTION OF THE MULTIPOLE PHASE ANGLES

The form of the transformed argument z' in the small-order approximation suggests that the general case may be analyzed in terms of the modulus and phase factors of the Riccati-Bessel functions. We accordingly define

$$\psi_n(z)=M_n(z)\sin\vartheta_n(z),\quad \chi_n(z)=-M_n(z)\cos\vartheta_n(z), \tag{11a}$$

$$\psi_n'(z)=N_n(z)\cos\phi_n(z),\quad \chi_n'(z)=N_n(z)\sin\phi_n(z), \tag{11b}$$

which ensures that $\vartheta_0(z)=\phi_0(z)=z$, while $\psi_n(z),\psi_n'(z)\to 0$ for $n\to\infty$ requires $\vartheta_n(z)\to 0$ and $\phi_n(z)\to\pi/2$ when $n\to\infty$. The properties and relations between these factors are presented in Appendix A where it is shown that

$$\psi_n'(z)=\frac{\cos[\vartheta_n(z)+\Delta_n(z)]}{M_n(z)\cos\Delta_n(z)}, \tag{12a}$$

$$\chi_n'(z)=\frac{\sin[\vartheta_n(z)+\Delta_n(z)]}{M_n(z)\cos\Delta_n(z)}, \tag{12b}$$

where $\Delta_n(z)=\phi_n(z)-\vartheta_n(z)$. Substitution of the above expressions in to Eqs. (3) then yields

$$\tan\begin{Bmatrix}u_n\\v_n\end{Bmatrix}=\frac{a\tan\vartheta_n(\beta)-b\tan\vartheta_n(\alpha)-c\tan\vartheta_n(\alpha)\tan\vartheta_n(\beta)}{c\tan\vartheta_n(\beta)+a\tan\vartheta_n(\alpha)\tan\vartheta_n(\beta)+b}, \tag{13}$$

in which for

$$u_n:\quad a=m/M_n^2(\alpha),\quad b=1/M_n^2(\beta);$$
$$v_n:\quad a=1/M_n^2(\alpha),\quad b=m/M_n^2(\beta);$$

and $c=a\tan\Delta_n(\alpha)-b\tan\Delta_n(\beta)$. By further manipulation (see Appendix B) the form of Eq. (13) can be reduced to

$$\tan\begin{Bmatrix}u_n\\v_n\end{Bmatrix}=\frac{\sigma\tan[\vartheta_n(\beta)+\tau]-\tan[\vartheta_n(\alpha)+\rho]}{1+\sigma\tan[\vartheta_n(\beta)+\tau]\tan[\vartheta_n(\alpha)+\rho]}, \tag{14}$$

where for

$$u_n:\quad \sigma=e^{\kappa},\quad \tan\tau=e^{-\lambda};$$
$$v_n:\quad \sigma=e^{-\kappa},\quad \tan\tau=-e^{\lambda};$$

and $\cosh\kappa=(a^2+b^2+c^2)/2ab$, $\sinh\lambda=(a^2-b^2+c^2)/2bc$, and $\tan\rho=\sigma\tan\tau$. The expressions for σ apply when $m>1$; for $m<1$ the signs of κ should be reversed. The phase angles can now be written as

$$\begin{Bmatrix}u_n\\v_n\end{Bmatrix}=\vartheta_n(\beta)-\vartheta_n(\alpha)+\tan^{-1}\left\{\frac{(\sigma-1)\tan[\vartheta_n(\beta)+\tau]}{1+\sigma\tan^2[\vartheta_n(\beta)+\tau]}\right\}-(\rho-\tau), \tag{15}$$

giving a dominant component

$$\begin{Bmatrix}\bar{u}_n\\\bar{v}_n\end{Bmatrix}=\vartheta_n(\beta)-\vartheta_n(\alpha) \tag{16}$$

and increment

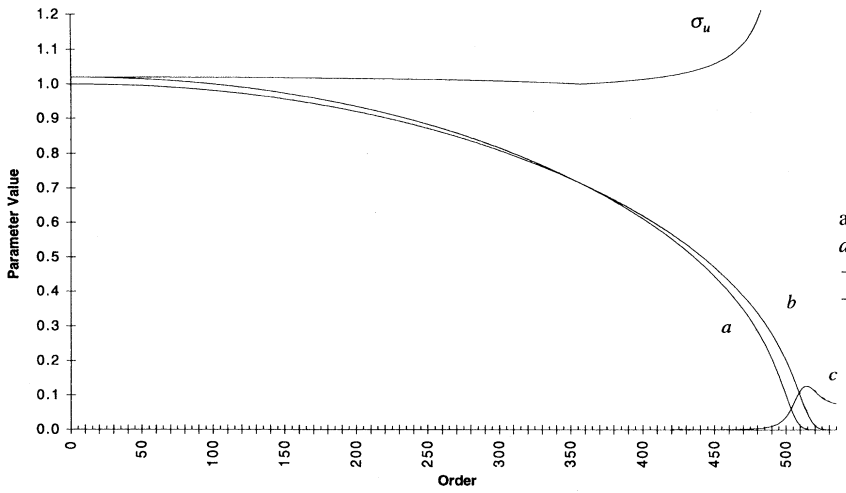

FIG. 3. Parameters of electric multipole phase angle u_n for $\alpha=500.5$, $\beta=510.5$, and $m=1.02$. $a=m/M_n^2(\alpha)$, $b=1/M_n^2(\beta)$, $c=a\tan\Delta_n(\alpha)-b\tan\Delta_n(\beta)$, and $\sigma_u=e^{\kappa}$, where $\cosh\kappa=(a^2+b^2+c^2)/2ab$.

$$\begin{Bmatrix}\tilde{u}_n\\ \tilde{v}_n\end{Bmatrix}=\tan^{-1}\left\{\frac{(\sigma-1)\tan[\vartheta_n(\beta)+\tau]}{1+\sigma\tan^2[\vartheta_n(\beta)+\tau]}\right\}-\tan^{-1}\left\{\frac{(\sigma-1)\tan\tau}{1+\sigma\tan^2\tau}\right\} \quad (17)$$

by eliminating ρ. Both incremental terms have their principal values and lie in the range $-\pi/2$ to $+\pi/2$. The choice of the expressions contributing to the dominant and incremental components is made to match the behavior of the principal and secondary structures, respectively, of Figs. 1 and 2. Thus $\tilde{u}_n=\tilde{v}_n$ start at $\vartheta_0(\beta)-\vartheta_0(\alpha)=\beta-\alpha$ and reduce monotonically to zero with increasing order. The remaining terms of Eq. (15) then make up the incremental component such that $\tilde{u}_n\neq\tilde{v}_n$. Furthermore, $\tilde{u}_n$ and $\tilde{v}_n$ yield the incremental parts of Eqs. (7) and (10), oscillate rapidly with order, and meet the requirements $\tilde{u}_n,\tilde{v}_n\to 0$ when $n\to\infty$.

Our modulus and phase factors are closely related to those of Bessel functions [6] and may be determined from

$$M_n^2(z)=1+\frac{1}{2}\frac{\mu_1}{z^2}+\frac{1\times3}{2\times4}\frac{\mu_1\mu_2}{z^4}+\frac{1\times3\times5}{2\times4\times6}\frac{\mu_1\mu_2\mu_3}{z^6}+\cdots, \quad (18)$$

$$\vartheta_n(z)=z-n\frac{\pi}{2}+\frac{\mu_1}{2z}+\frac{\mu_1(\mu_1-6)}{24z^3}+\frac{\mu_1(\mu_1^2-28\mu_1+60)}{80z^5}+\frac{\mu_1(5\mu_1^3-380\mu_1^2+3228\mu_1-5040)}{896z^7}+\cdots, \quad (19)$$

$$\tan\Delta_n(z)=\frac{\mu_1}{2z^3}\left\{1+\frac{3}{2}\frac{\mu_2}{z^2}+\frac{3\times5}{2\times4}\frac{\mu_2\mu_3}{z^4}+\frac{3\times5\times7}{2\times4\times6}\frac{\mu_2\mu_3\mu_4}{z^6}+\cdots\right., \quad (20)$$

in which $\mu_p=(n+p)(n-p+1)$. When applied to the small-order approximation Eqs. (6), (17), and (19), together with $\tau=0$, and $\sigma=m$ for u_n and $\sigma=1/m$ for v_n, lead to phase angles in agreement with Eqs. (10).

IV. APPLICATIONS

Our analysis is valid for all nonabsorbing spheres and may be used to investigate the behavior of various parameters defined in the treatment as a function of order. Such parameters turn out to be nonoscillatory, unlike the behavior of a_n and b_n. An exception to this is the contribution of the phase increment arising from the term containing $\tan\{\vartheta_n(\beta)+\tau\}$. No restriction is present on the particle size in the treatment, but for small particles plots against order will be sparse in data points and any systematic trends may be less discernible. Accordingly, we chose to investigate a large sphere of fixed size $\alpha=500.5$ but vary β so as to illustrate the behavior of three classes of particle: $\beta>\alpha$, $\beta\to\alpha$, and $\beta<\alpha$.

A. Case A: $\beta>\alpha$, $m>1$

Results for a, b, c, and σ for u_n and v_n of a sphere with $\alpha=500.5$, $\beta=510.5$, and $m=1.02$ are given in Figs. 3 and 4, whereas Fig. 5 shows the corresponding values of τ. The typical monotonic variation of $1/M_n^2(z)$ against order with a cutoff at $n\geq z$ is shown by curve b of Fig. 3 and curve a of Fig. 4. The value of c, on the other hand, remains very small until a threshold is reached below $n=\alpha$ when it raises to a peak at $n\approx\beta$.

To explain the features of Fig. 5 we note that when $b^2=a^2+c^2$, $\lambda=0$ to give $\tau_u=\pi/4$ or $\tau_v=-\pi/4$. This condition first arises in Fig. 3 when a and b cross at $n\approx\{m\alpha/\sqrt{1+m^2}\}-\frac{1}{2}=357$, obtained by applying approximation (A16). Below the crossing point $a>b$ and $c\approx0$, yielding a large positive value of λ so that $\tau_u\approx0$, but above the crossing λ is large and negative, giving $\tau_u\approx\pi/2$. Thus τ_u undergoes a sharp upward transition $0\to\pi/2$ at $n=357$. A second occurrence of the condition $b^2=a^2+c^2$ is found in Fig. 3 at $n=505$ just before the crossing of b and c. This marks a second transition of τ_u from $\pi/2$ to 0, the final value being ensured by $a\to0$ and $b\to0$. Only the latter crossing is present in Fig. 4. In this case, $b>a$ and $c\approx0$ below $n=505$ so that λ is large and negative and τ_v has a small negative value. Above $n=505$, a and b reduce with increasing order

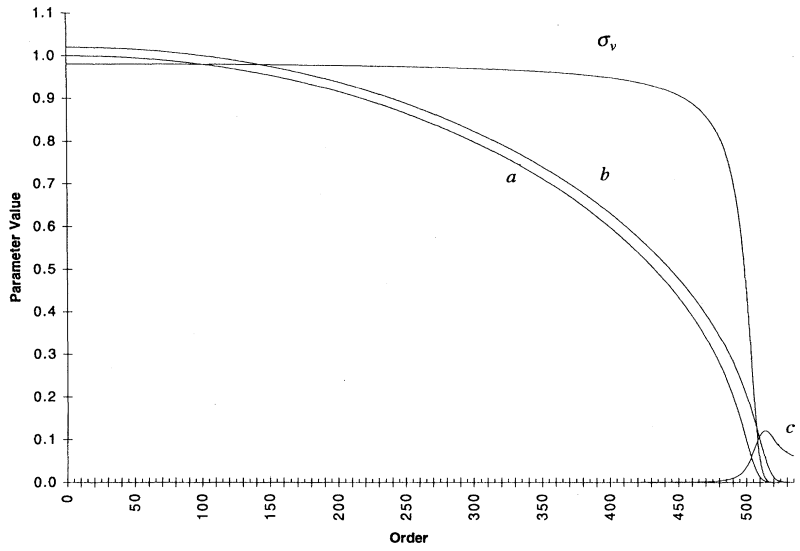

FIG. 4. Parameters of magnetic multipole phase angle ν_n for $\alpha=500.5$, $\beta=510.5$, and $m=1.02$. $a=1/M_n^2(\alpha)$, $b=m/M_n^2(\beta)$, $c=a\tan\Delta_n(\alpha)-b\tan\Delta_n(\beta)$, and $\sigma_v=e^{-\kappa}$, where $\cosh\kappa=(a^2+b^2+c^2)/2ab$.

and λ becomes large and positive to yield a final value of $\tau_v=-\pi/2$.

A notable feature of Fig. 3 is the minimum of σ_u at the crossing point of a and b at $n=357$. This arises since initially, $\sigma_u=m=1.02$, while at the crossing $\cosh\kappa=\sqrt{1+c^2/a^2}$, $\kappa\approx 0$, and $\sigma_u\approx 1$. Above $n=357$, both κ and σ increase as a and b reduce. In contrast, σ_v, of Fig. 4 starts at $\sigma_v=1/m=0.98$ and reduces monotonically to zero with a cutoff that coincides with that of curve a.

In order to discuss the incremental angles $\tilde{u}_n$ and $\tilde{v}_n$, we first define the separate components by

$$\epsilon_1=\tan^{-1}\left\{\frac{(\sigma-1)\tan[\vartheta_n(\beta)+\tau]}{1+\sigma\tan^2[\vartheta_n(\beta)+\tau]}\right\}, \tag{21a}$$

$$\epsilon_2=\tan^{-1}\left\{\frac{(\sigma-1)\tan\tau}{1+\sigma\tan^2\tau}\right\}. \tag{21b}$$

These are plotted in Fig. 6 for $\tilde{u}_n$. The first component is oscillatory and has an envelope curve of

$$\epsilon_1^b=\pm\tan^{-1}\{\sinh\kappa/2\} \tag{22}$$

whenever $\tan[\vartheta_n(\beta)+\tau]=\pm 1/\sqrt{\sigma}$. Thus the amplitude of $\epsilon_{1,u}^b$ initially decreases to zero at $n=357$, where $\kappa_u=0$, before increasing to $\pi/2$ at high orders. Within the bounds, $\epsilon_{1,u}$ is seen to reduce in periodicity with increasing orders. This is accounted for by the dependence of $\vartheta_n(\beta)$ on order. At low orders a change of order of 4 will cause $\vartheta_n(\beta)$ to reduce by 2π, but for higher orders Δn will continually increase to obtain the same reduction in $\vartheta_n(\beta)$. The component ϵ_2 can be expressed in the form

$$\epsilon_2=\tan^{-1}\left[\frac{\sinh(\kappa/2)}{\cosh\{(\kappa/2)-\lambda\}}\right], \tag{23}$$

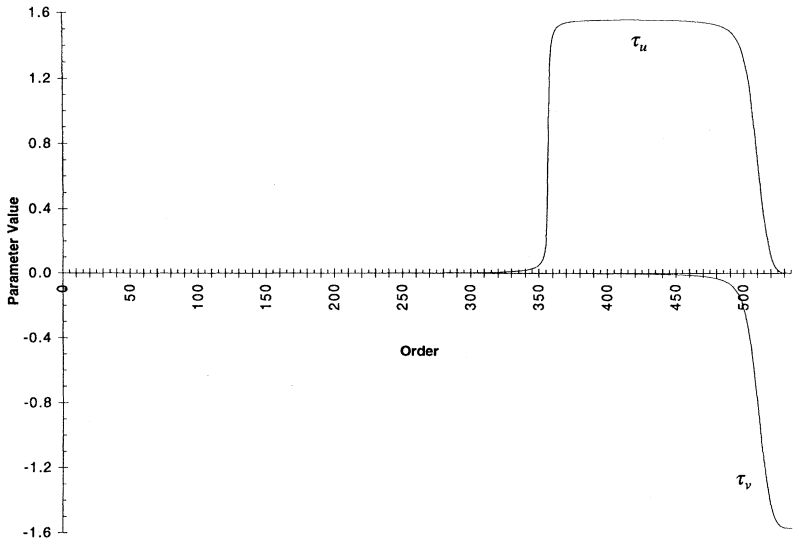

FIG. 5. Variation of τ_u and τ_v with order for $\alpha=500.5$, $\beta=510.5$, and $m=1.02$. $\tan\tau_u=e^{-\lambda_u}$ and $\tan\tau_v=-e^{\lambda_v}$, where $\sinh\lambda=(a^2-b^2+c^2)/2bc$.

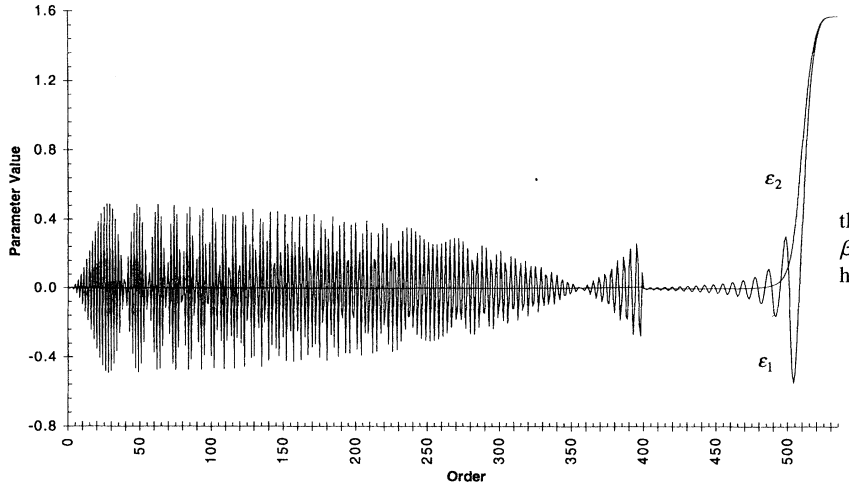

FIG. 6. Variation of ϵ_1 and ϵ_2 components of the incremental angle $\tilde{u}_n$ with order for $\alpha=500.5$, $\beta=510.5$, and $m=1.02$. Values below $n=400$ have been magnified by a factor of 20.

It is therefore always smaller than the positive limit of ϵ_1^b. Below the threshold of c, ϵ_2 is negligible because either $|\lambda|$ is large or $\kappa=0$. However, on passing the threshold of c, ϵ_2 rises to coincide with ϵ_1 at a final value of $\pi/2$. Plots similar to Fig. 6 are obtained for the incremental components of $\tilde{v}_n$, except that the amplitude component of the envelope curve continuously increases with order.

When the dominant component is combined with the incremental, we obtain the total phase angles u_n and v_n, which are illustrated in Fig. 7. The predominant behavior of these plots is determined by the monotonic decrease of $\vartheta_n(\beta)-\vartheta_n(\alpha)$ from the initial values $u_0\approx v_0\approx\beta-\alpha$. A significant difference between these two curves exists, however, due to the reduction to zero and subsequent growth of $\tilde{u}_n$ as $n=357$ is approached and passed. At high orders the amplitudes of the increments grow, but can never exceed the dominant term. The largest negative contribution of the increment is found at $n=500.5$ when $\vartheta_n(\beta)\approx 1.43$, obtained from $\vartheta_n(\beta)=\pi-\tau_u-\tan^{-1}(1/\sqrt{\sigma_u})$ or $\vartheta_n(\beta)=\tan^{-1}(1/\sqrt{\sigma_v})-\tau_v$. Its presence has the effect of advancing the cutoff order of the phase angle from that expected from the dominant term alone. The values of u_n and v_n may be used to directly calculate the Mie coefficients of a_n and b_n by applying Eqs. (4). As the original refractive index is quite close to unity, spheres with larger values of m were also examined. No new features were found in the behavior of a,b,c,σ,τ, or ϵ_2. An additional development, however, was observed for ϵ_1 in the range $\alpha<n<\beta$. This took the form of sawtooth oscillations with peak-to-peak magnitudes of π. As a consequence, a rectangular staircase with steps of height π but varying widths was generated in the plots of the total phase u_n and v_n. An example of such a staircase can be seen in Fig. 8(D) for $u_n/(\beta-\alpha)$ of a particle having $\alpha=500.5$, $\beta=550.5$, and $m=1.10$. It should be noted that all the steps shown in Fig. 8 have been scaled in height by the normalization factor. With hindsight, we now see that the phase angle of our origi-

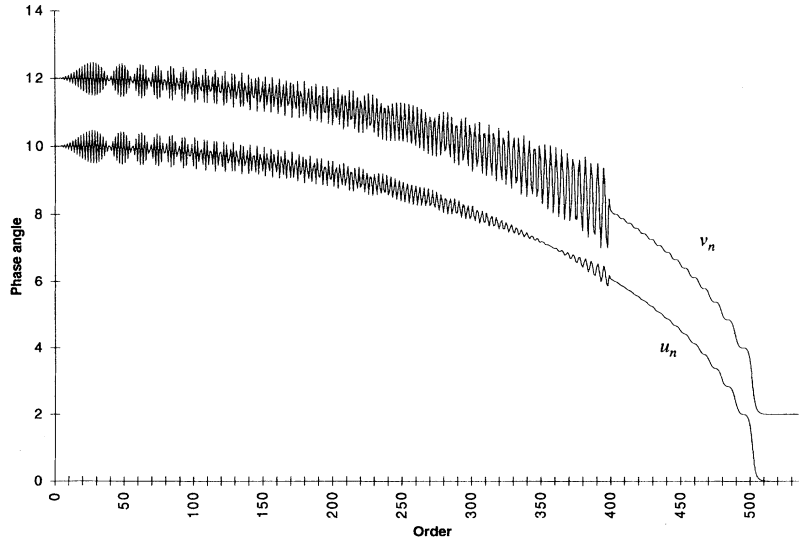

FIG. 7. Comparison of phase angles u_n and v_n for $\alpha=500.5$, $\beta=510.5$, and $m=1.02$. Values below $n=400$ have been magnified by a factor of 20 and v_n has a plotting increment of $+2.0$.

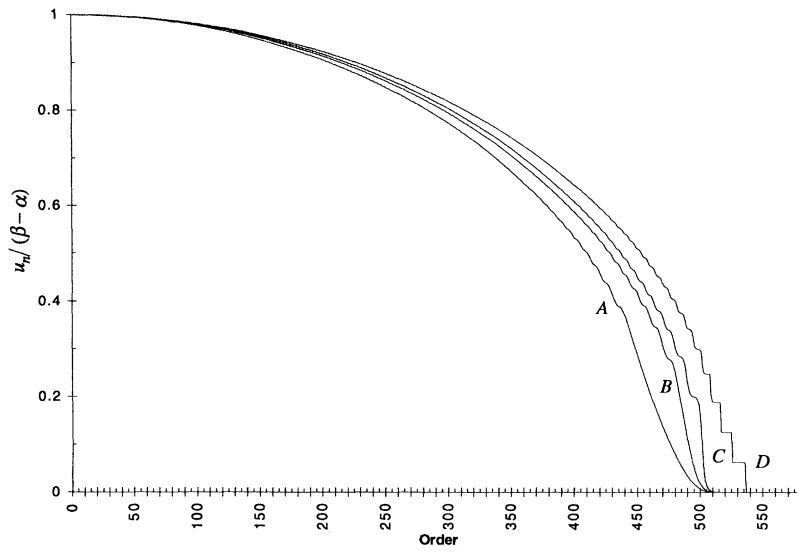

FIG. 8. Variation of normalized phase angle u_n with order. (A) $\alpha=500.5$, $\beta=450.5$, and $m=0.90$; (B) $\alpha=500.5$, $\beta=490.5$, and $m=0.98$; (C) $\alpha=500.5$, $\beta=510.5$, and $m=1.02$; and (D) $\alpha=500.5$, $\beta=550.5$, and $m=1.10$.

nal particle, curve C, approaches its cutoff by a sequence of embryonic steps, which are partially developed in height and profile.

A qualitative explanation of the origin of the steps can be obtained by modifying Eq. (14a) into

$$\tan u_n=\frac{\psi_n(\alpha)}{\chi_n(\alpha)}\left\{\frac{\dfrac{\psi_n'(\beta)}{\psi_n(\beta)}-m\dfrac{\psi_n'(\alpha)}{\psi_n(\alpha)}}{\dfrac{\psi_n'(\beta)}{\psi_n(\beta)}-m\dfrac{\chi_n'(\alpha)}{\chi_n(\alpha)}}\right\}. \tag{24}$$

For values of $n>\alpha$, $\psi_n(\alpha)/\chi_n(\alpha)\to 0$ but the term in the large curly brackets continues to change sign as n increases. Hence the solution of the equation is $u_n=p\pi$, where p is an integer and the steps will occur each time the denominator in the large curly brackets passes through zero. A similar treatment can be applied to v_n. In terms of our formulation, the condition equivalent to $\psi_n(\alpha)/\chi_n(\alpha)\to 0$ is $\sigma\to\infty$ for u_n and by Eq. (17) we obtain

$$\begin{aligned}\tilde{u}_n&=\tan^{-1}\left\{\frac{1}{\tan[\vartheta_n(\beta)+\tau_u]}\right\}-\tan^{-1}\left\{\frac{1}{\tan\tau_u}\right\}\\&=p\pi-\vartheta_n(\beta),\quad \tau_u-\pi\le u_n\le\tau_u.\end{aligned} \tag{25}$$

Discontinuities then arise whenever $\vartheta_n(\beta)=p\pi-\tau_u$. In the case of $v_n,\sigma_v\to 0$ and

$$\tilde{v}_n=p\pi-\vartheta_n(\beta),\quad \tau_v-\pi/2\le\tilde{v}_n\le\pi/2+\tau_v, \tag{26}$$

giving steps when $\vartheta_n(\beta)=(p+1/2)\pi-\tau_v$. Thus, for $n>\alpha$ the total phase takes the form of a descending staircase

$$\begin{Bmatrix}u_n\\v_n\end{Bmatrix}=p\pi-\vartheta_n(\alpha), \tag{27}$$

which has a cutoff at an order obtained from $\vartheta_n(\beta)=\pi-\tau_u$ for u_n and $\vartheta_n(\beta)=\pi/2-\tau_v$ for v_n.

B. Case B: $\beta\to\alpha$, $m-1\to 0$

The limiting case of the relative refractive index approaching unity corresponds to that of the Rayleigh-Debye sphere. For such a particle with $\beta\to\alpha=500.5$, the characteristics of the parameters are generally similar to Figs. 3–5 except that a and b are indistinguishable, while c is greatly reduced in magnitude and has a sharp peak at $n=510$. The principle effects of these differences are that both σ_u and σ_v remain close to unity for $n<\alpha$ and the largest negative peaks of $\tilde{n}_n$ and $\tilde{u}_n$ are at $n=418$. Under the above conditions, the dominant component of the phase angles is approximated by

$$\begin{Bmatrix}\tilde{u}_n\\\tilde{v}_n\end{Bmatrix}\approx(\beta-\alpha)\vartheta_n'(\alpha)=\frac{(\beta-\alpha)}{M_n^2(\alpha)} \tag{28}$$

on using Eq. (A10). Furthermore,

$$\begin{Bmatrix}\tilde{u}_n\\\tilde{v}_n\end{Bmatrix}\approx(\sigma-1)\{\cos[2\vartheta_n(\alpha)+2\tau]-\cos 2\tau\} \tag{29}$$

for $n<\alpha$.

Solutions of the phase angles can also be obtained by reducing the Mie equations in the Rayleigh-Debye limit of $\gamma=(m^2-1)\alpha/2\approx\beta-\alpha\ll 1$ [4]. These are

$$u_n=\frac{\gamma\bar{f}_n^1(\alpha)}{1+\dfrac{2n\gamma}{(2n+1)\alpha}}, \tag{30a}$$

$$v_n=\gamma f_n^1(\alpha), \tag{30b}$$

where $f_n^1(\alpha)=\psi_n^2(\alpha)-\psi_{n+1}(\alpha)\psi_{n-1}(\alpha)$ and $\bar{f}_n^1(\alpha)=f_n^1(\alpha)+2\psi_n(\alpha)\psi_n'(\alpha)/\alpha$. However, because of the large particle size in the present case, Eq. (30a) may be simplified to

$$u_n=\gamma\bar{f}_n^1(\alpha). \tag{30c}$$

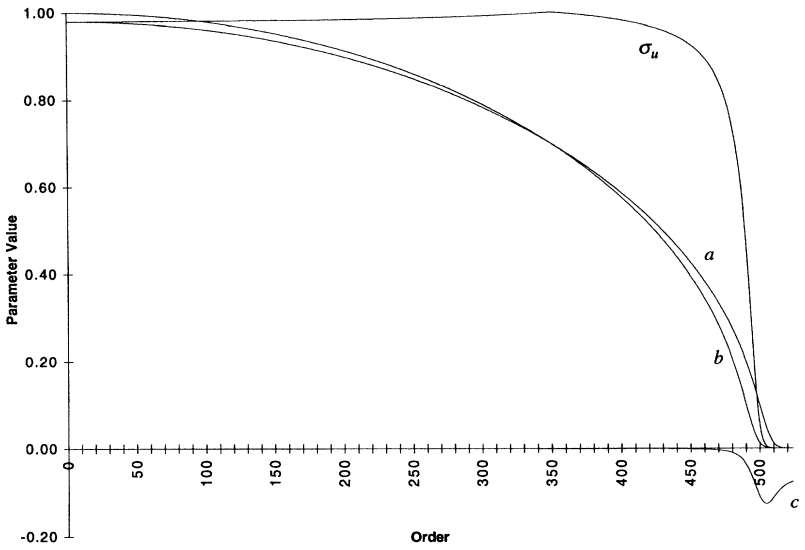

FIG. 9. Parameters of electric multipole phase angle u_n for $\alpha=500.5$, $\beta=490.5$, and $m=0.98$. $a=m/M_n^2(\alpha)$, $b=1/M_n^2(\beta)$, $c=a\tan\Delta_n(\alpha)-b\tan\Delta_n(\beta)$, and $\sigma_u=e^{-\kappa}$, where $\cosh\kappa=(a^2+b^2+c^2)/2ab$.

The combination of Eqs. (30) and (28) then yields expressions for the incremental angles,

$$\tilde{u}_n=\gamma\left[\tilde{f}_n^1(\alpha)-\frac{1}{M_n^2(\alpha)}\right], \tag{31}$$

$$\tilde{v}_n=\gamma\left[f_n^1(\alpha)-\frac{1}{M_n^2(\alpha)}\right], \tag{32}$$

since $\sigma\approx 1$. The cutoff orders may be found from $\vartheta_n(\alpha)=(3\pi/4)-\tau_u$ for u_n and $\vartheta_n(\alpha)=(\pi/4)-\tau_v$ for v_n.

Particular formulas can be derived for σ and $\sinh\lambda$ by expanding $\tilde{f}_n^1(\alpha)$ and $f_n^1(\alpha)$ of Eqs. (31) in modulus and phase factors and comparing the resulting expressions with Eq. (29). This leads to

$$\sigma_u=1+\gamma\{[A+B_u\tan\Delta_n(\alpha)]^2+B_u^2\}^{1/2}, \tag{33a}$$

$$\sigma_v=1-\gamma\{[A-B_v\tan\Delta_n(\alpha)]^2+B_v^2\}^{1/2}, \tag{33b}$$

$$\sinh\lambda_u=\frac{B_u}{A+B_u\tan\Delta_n(\alpha)}, \tag{34a}$$

$$\sinh\lambda_v=\frac{-B_v}{A-B_v\tan\Delta_n(\alpha)}, \tag{34b}$$

where

$$A=\frac{1+\tan^2\Delta_n(\alpha)}{M_n^2(\alpha)}-\left[1-\frac{n(n+1)}{\alpha^2}\right]M_n^2(\alpha),$$

$$B_u=\frac{1}{\alpha}-\frac{2\tan\Delta_n(\alpha)}{M_n^2(\alpha)},$$

and

$$B_v=\frac{1}{\alpha}+\frac{2\tan\Delta_n(\alpha)}{M_n^2(\alpha)}.$$

These are valid when $n<\alpha$.

C. Case C: $\beta<\alpha$, $m<1$

Specimens belonging to this category have a lower refractive index than that of the ambient medium such as an air bubble in water. It is characteristic of the class that the phase angle and the parameter c are both negative. Curves of the various parameters are presented in Figs. 9–11 for $\alpha=500.5$, $\beta=490.5$, and $m=0.98$. The condition $b^2=a^2+c^2$ is now satisfied only for u_n at $n=350$, where a and b cross in Fig. 9. This marks the $0\rightarrow\pi/2$ transition of τ_u shown in Fig. 11. At orders greater than $n=350$, τ_u remains at $\pi/2$ while either b or c is small. However, between the threshold of c and the cutoff of b, $450<n<510$, both parameters are nonzero so that τ_u drops below $\pi/2$. As no transition is present for $v_n, \tau_v=0$ except between the overlap of c and b where a negative dip is generated. The variation of σ_u and σ_v with order is included in Figs. 9 and 10, respectively. From a starting value of $\sigma_u=m=0.98, \sigma_u$ initially rises to unity at the crossover of a and b before reducing to zero as the cutoff of b is approached. In contrast, σ_v has an initial value of $\sigma_v=1/m=1.02$ and grows continuously with increasing order.

Since the definitions of σ are now different from case A, the expression equivalent to Eq. (23) is

$$\epsilon_2=-\tan^{-1}\left[\frac{\sinh\kappa/2}{\cosh(\kappa/2+\lambda)}\right]. \tag{35}$$

Hence, at high orders ϵ_1 and ϵ_2 have limiting values of $-\pi/2$, as can be seen from Fig. 12 for u_n. Other features of the oscillatory component of $\tilde{u}_n$ are the reduction of its amplitude to zero at $n=350$ and the termination of the oscillation on a positive peak at $n=490$. The order of the last peak may be obtained from $\vartheta_n(\beta)=\pi-\tau-\tan^{-1}(1/\sqrt{\sigma})$, while that of the preceding negative peak is $\vartheta_n(\beta)=\pi-\tau+\tan^{-1}(1/\sqrt{\sigma})$. Accordingly, when the incremental and dominant components of the phase are combined in Fig. 13,

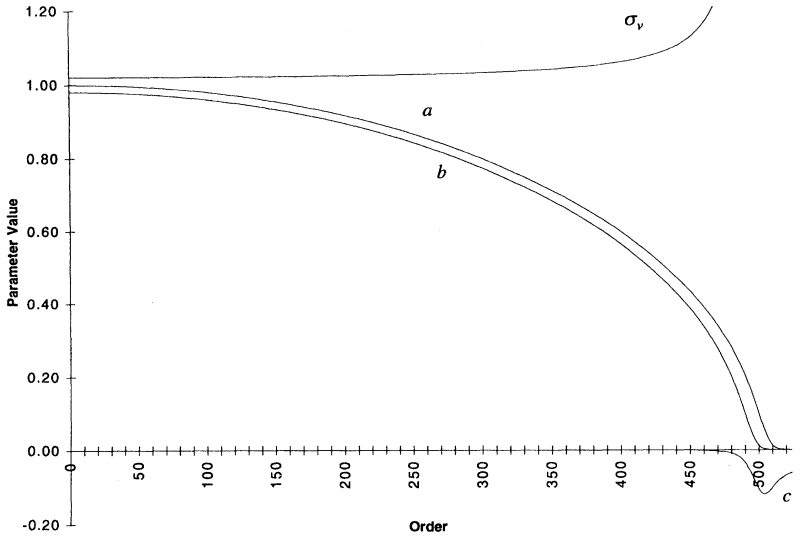

FIG. 10. Parameters of multipole phase angle v_n for $\alpha=500.5$, $\beta=490.5$, and $m=0.98$. $a=1/M_n^2(\alpha)$, $b=m/M_n^2(\beta)$, $c=a\tan\Delta_n(\alpha)-b\tan\Delta_n(\beta)$, and $\sigma_v=e^{\kappa}$, where $\cosh\kappa=(a^2+b^2+c^2)/2ab$.

the last evidence of oscillatory behavior in the phase angles is found close to the order of the last negative peak in ϵ_1 at $n=475$. This order may be obtained from $\vartheta_n(\beta)=\pi-\tau_u+\tan^{-1}(1/\sqrt{\sigma})$ for u_n or $\vartheta_n(\beta)=\pi-\tau_v-\tan^{-1}(1/\sqrt{\sigma})$ for v_n. At orders greater than $n=475$, the total phase angles increase monotonically to the cutoff of $\vartheta_n(\alpha)$. In general, the monotonic tails of the phase angles extend beyond the range $\beta<n<\alpha$. This is shown in curves A and B of Fig. 8 for $\alpha=500.5$ with $\beta=450.5$ and 490.5, respectively.

V. DISCUSSION

The complex Mie scattering coefficients a_n and b_n of a homogeneous sphere, which are dependent only on its size parameters α and β, may be expressed in terms of real electric and magnetic multipole phase angles u_n and v_n, respectively. However, to obtain the phase angles, the trigonometric functions of Eq. (3) require inversion and yield values only within the range $-\pi/2$ to $\pi/2$. Nevertheless, cases do exist where inversion leads to absolute values of angles. An example is the phase angle in the modulus and phase factors of Bessel functions. It is therefore a basic assumption of our analysis that the phase angles u_n and v_n can be usefully defined by their absolute values as a function of order.

The method originally used in Sec. II for finding u_n and v_n from the variation of a_n and b_n with order is not generally satisfactory. Accordingly, Eqs. (16) and (17) should be adopted for inverting $\tan u_n$ and $\tan v_n$ when α and β are known. The equations, however, require the evaluation of the modulus and phase factors of Riccati-Bessel functions. $M_n^2(z)$ and $\tan\Delta_n(z)$ may be determined from Eqs. (18) and (20) or Eqs. (A4) and (A11), but accurate values of $\vartheta_n(z)$ can only be generated in the range $-\pi/2$ to $+\pi/2$ by Eq. (A5). An absolute specification of $\vartheta_n(z)$ is possible by the

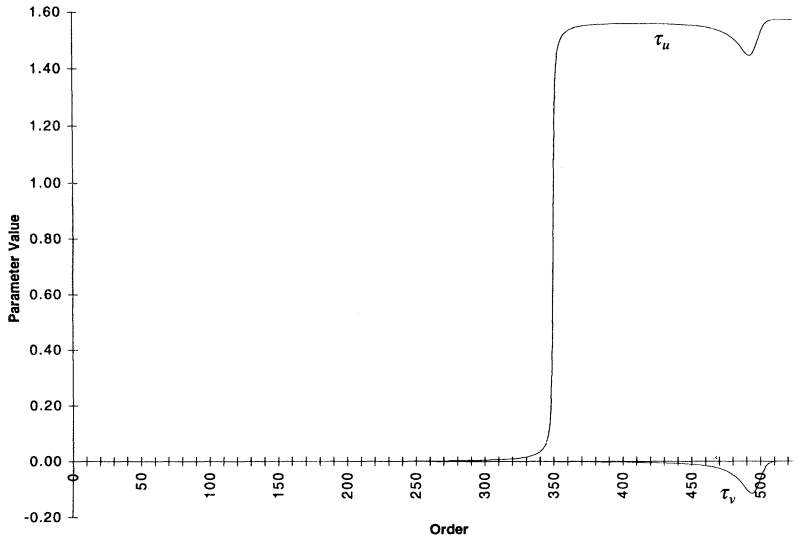

FIG. 11. Variation of τ_u and τ_v with order for $\alpha=500.5$, $\beta=490.5$, and $m=0.98$. $\tan\tau_u=e^{-\lambda_u}$ and $\tan\tau_v=-e^{\lambda_v}$, where $\sinh\lambda=(a^2-b^2+c^2)/2bc$.

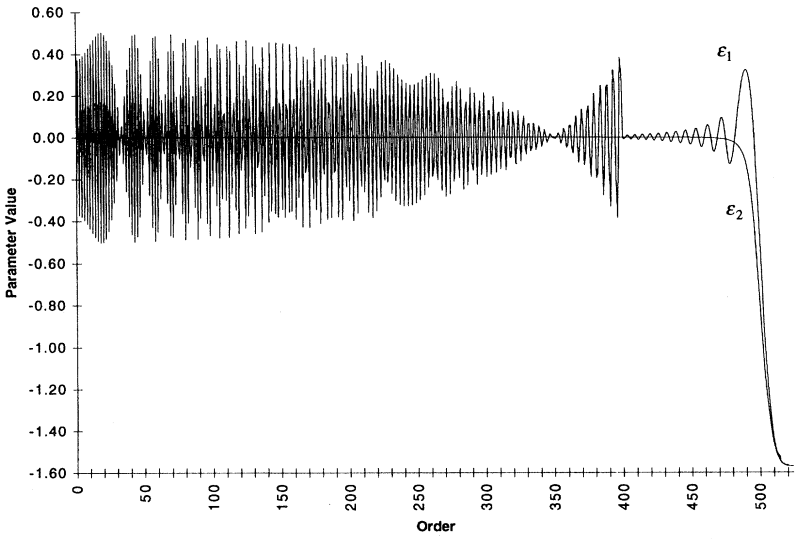

FIG. 12. Variation of ϵ_1 and ϵ_2 components of the incremental angle $\tilde{u}_n$ with order for $\alpha=500.5$, $\beta=490.5$, and $m=0.98$.

following convention. The angle at zeroth order is first found from $\vartheta_0(z)=z$. For succeeding adjacent orders, the angles are then obtained by shifting $\vartheta_n(z)$ to the next lowest quadrant when its tangent changes sign. If no change of sign occurs, the angle lies in the same quadrant as that of the preceding order. When u_n and v_n are obtained, the numerical values of a_n and b_n can be calculated from Eqs. (4).

An analysis of the variation of the phase angles with order has shown that the angles can be separated into dominant $\bar{u}_n,\bar{v}_n$ and incremental $\tilde{u}_n,\tilde{v}_n$ components: $u_n=\bar{u}_n+\tilde{u}_n$ and $v_n=\bar{v}_n+\tilde{v}_n$. The separation is effected by replacing the Riccati-Bessel functions of the Mie's treatment by their modulus and phase factors. This leads to expressions that contain $\vartheta_n(\alpha),\vartheta_n(\beta),\sigma$, and τ. The last two parameters, which vary with α, β, and n, are derived from quadratic equations and have different definitions for electric and magnetic multipole terms. As a result, $0\leq\tau_u\leq\pi/2$ and $-\pi/2\leq\tau_v\leq 0$, but $\sigma_u>1$ and $\sigma_v<1$ when $\beta>\alpha$, and $\sigma_u<1$ and $\sigma_v>1$ for $\beta<\alpha$. The dominant component is the same for both types of phase and reduce monotonically to zero with increasing order according to $\bar{u}_n=\bar{v}_n=\vartheta_n(\beta)-\vartheta_n(\alpha)$. On the other hand, the incremental components are different and oscillate as a function of order given by

$$\begin{Bmatrix}\tilde{u}_n\\ \tilde{v}_n\end{Bmatrix}=\tan^{-1}\left\{\frac{(\sigma-1)\tan[\vartheta_n(\beta)+\tau]}{1+\sigma\tan^2[\vartheta_n(\beta)+\tau]}\right\}-\tan^{-1}\left\{\frac{(\sigma-1)\tan\tau}{1+\sigma\tan^2\tau}\right\}.$$

The difference arises from the alternative definitions of σ and τ. In the case of v_n, the oscillations are constrained within an envelope that grows with order until termination before $n=\beta$, but for u_n, the growth of the oscillation is ini-

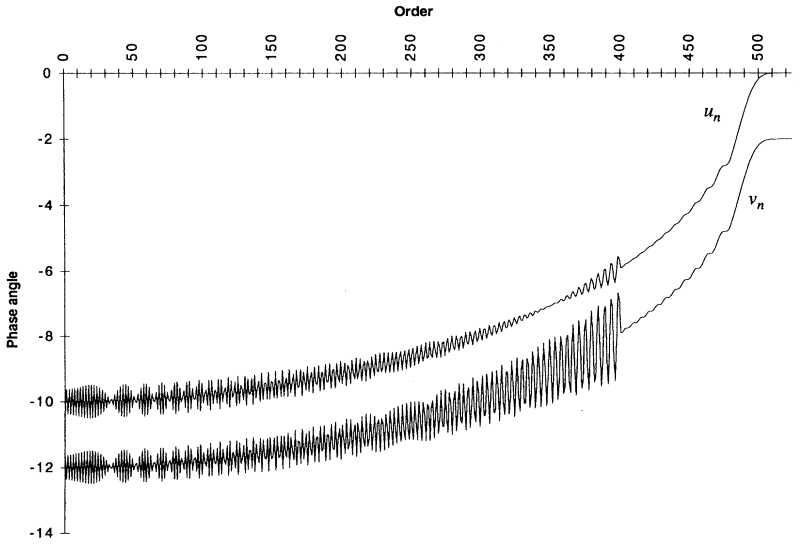

FIG. 13. Comparison of phase angles u_n and v_n for $\alpha=500.5$, $\beta=490.5$, and $m=0.98$. Values below $n=400$ have been magnified by a factor of 20 and v_n has a plotting increment of -2.0.

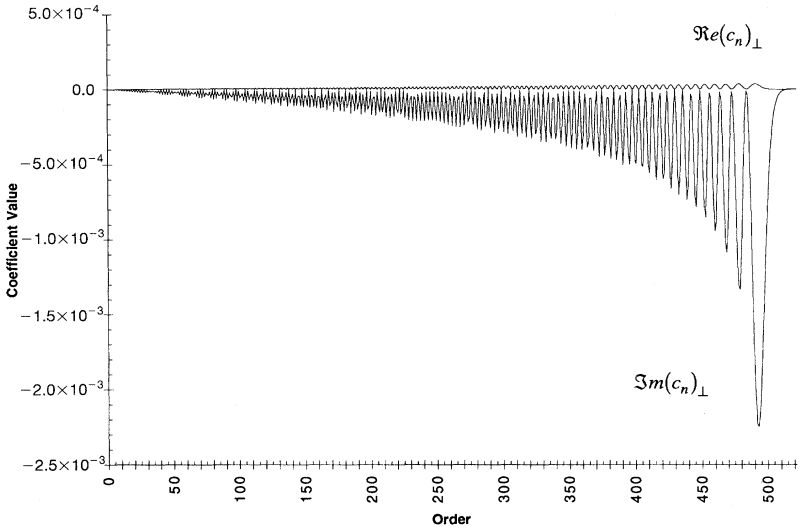

FIG. 14. Variation of $\mathrm{Re}(c_n)_\perp$ and $\mathrm{Im}(c_n)_\perp$ with order for $\alpha=500.5$, $\beta=500.55$, and $m=1.0001$.

tially suppressed by a requirement that the amplitude of the envelope reduce to zero at $n\approx\{m\alpha/\sqrt{1+m^2}\}-1/2$ when $M_n^2(\alpha)\approx mM_n^2(\beta)$.

Plots of the multipole phase angles are also compared when α is held constant and β is varied. For $\beta/\alpha<0.98$, the oscillations of the incremental components of u_n and v_n terminate near $n=\beta$ to leave a monotonic tail with a cutoff just above $n=\alpha$. At the opposite limit of $\beta/\alpha>1.02$, the phase angles become quantized in units of π for $n>\alpha$ to generate a staircase function with a cutoff order before $n=\beta$. The phenomenon, however, leads to no detectable experimental effects since $a_n=b_n=0$ for quantized phase angles. Thus, for all values of β, a_n, and b_n have cutoff orders at $n\geqslant\alpha$.

From the alternative formulation of Mie scattering given by Eq. (1b), the a_n and b_n scattering coefficients can be replaced by Gegenbauer coefficients $(c_n)_\perp$ and $(c_n)_\parallel$ for perpendicular and parallel polarization. These coefficients may also be written in terms of the phase angles by substituting Eqs. (4) into Eq. (2) to obtain

$$(c_n)_\perp=-i\left\{\frac{n}{n+1}\sin(v_n-u_{n+1})e^{i(v_n+u_{n+1})}+\frac{n+3}{n+2}\sin(u_{n+1}-v_{n+2})e^{i(u_{n+1}+v_{n+2})}\right\},\tag{36a}$$

$$(c_n)_\parallel=-i\left\{\frac{n}{n+1}\sin(u_n-v_{n+1})e^{i(u_m+v_{n+1})}+\frac{n+3}{n+2}\sin(v_{n+1}-u_{n+2})e^{i(v_{n+1}+u_{n+2})}\right\},\tag{36b}$$

Such formulas are simplified when applied to a large Rayleigh-Debye sphere for which $\gamma=\beta-\alpha\ll1$ and $\gamma/\alpha\ll1$. As a consequence, $u_n,v_n\to0$, yielding

$$(c_n)_\perp=-i\left\{\frac{n}{n+1}(v_n-u_{n+1})+\frac{n+3}{n+2}(u_{n+1}-v_{n+2})\right\}$$
$$=-i\gamma\left\{\frac{n}{n+1}[f_n^1(\alpha)-\bar{f}_{n+1}^1(\alpha)]+\frac{n+3}{n+2}[\bar{f}_{n+1}^1(\alpha)-f_{n+2}^1(\alpha)]\right\}\tag{37a}$$

and

$$(c_n)_\parallel=-i\left\{\frac{n}{n+1}(u_n-v_{n+1})+\frac{n+3}{n+2}(v_{n+1}-u_{n+2})\right\}$$
$$=-i\gamma\left\{\frac{n}{n+1}[\bar{f}_n^1(\alpha)-f_{n+1}^1(\alpha)]+\frac{n+3}{n+2}[f_{n+1}^1(\alpha)-\bar{f}_{n+2}^1(\alpha)]\right\}\tag{37b}$$

by using Eqs. (30b) and (30c). The identities $(2n+1)\bar{f}_n^1(\alpha)=(n+1)f_{n-1}^1(\alpha)+nf_{n+1}^1(\alpha)$ and $f_n^1(\alpha)-f_{n+2}^1(\alpha)=2(2n+3)j_{n+1}^2(\alpha)$ [4] are finally invoked to obtain

$$(c_n)_\perp=-i2\gamma(2n+3)j_{n+1}^2(\alpha),\tag{38a}$$

$$(c_n)_\parallel=-i2\gamma[nj_n^2(\alpha)+(n+3)j_{n+2}^2(\alpha)].\tag{38b}$$

The coefficients are in agreement with those derived from the Rayleigh-Debye scattering formulas when $\gamma/\alpha\to0$ [4]. Hence we can now see that the Rayleigh-Debye treatment is valid for the limiting case of $m-1\to0$. Such a condition ensures that both $\gamma\ll1$ and $\gamma/\alpha\ll1$. For small spheres where $\alpha\ll1$, the condition $\gamma\ll1$ only is insufficient to specify Rayleigh-Debye scattering and deviations can be present. This case has been discussed in Ref. [4], where for $\alpha<1$ it was shown that the scattering coefficients reduce to the Rayleigh-Debye form but contain additional weighting factors when γ/α is not negligible.

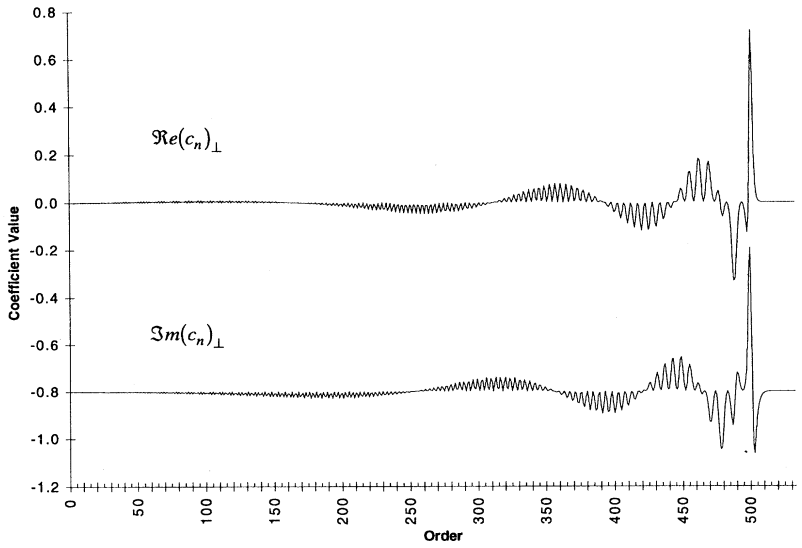

FIG. 15. Variation of $\mathrm{Re}(c_n)_\perp$ and $\mathrm{Im}(c_n)_\perp$ with order for $\alpha=500.5$, $\beta=510.5$, and $m=1.02$. The imaginary component has a plotting increment of -0.8.

Graphs of $(c_n)_\perp$ are shown in Figs. 14 and 15 for $\alpha=500.5$, $\beta=500.55$, and $m=1.0001$ and $\alpha=500.5$, $\beta=510.5$, and $m=1.02$, respectively. The first particle is a good approximation to a Rayleigh-Debye sphere since $\gamma=0.05$ and $\gamma/\alpha=10^{-4}$, but the second is not as $\gamma=10.1$ and $\gamma/\alpha=0.02$. Equation (38a) can therefore be used to explain the features of Fig. 14, although a small deviation from the expected behavior is present since $\mathrm{Re}(c_n)_\perp$ is small relative to $\mathrm{Im}(c_n)_\perp$ but not zero. When the relative refractive index of the sphere is increased, the simple structure of Fig. 14 develops new features as shown by Fig. 15. There are the growth of the real component so as to be comparable with the imaginary part and the appearance of modulated envelope curves of the two components that oscillate about zero with order.

The present analysis is applicable to all homogeneous dielectric spheres and, despite the complexity of the formulation, gives valuable insight into the behavior of the scattering coefficients as a function of order. Since a good estimate of α may be obtained from the Gegenbauer spectrum of the scattering pattern, it is anticipated that the main use of the above formulas will be in the search for algorithms that will allow the determination of β.

Our treatment is also directly applicable to absorbing homogeneous spheres, but the complex values of β would lead to complex expressions for $\vartheta_n(\beta), M_n(\beta)$, and $\Delta_n(\beta)$. The conditions for generalizing the present technique to other geometries are that the electric and magnetic phase angles of the specimen have the same forms as Eqs. (3) and involve functions that can be written as products of moduli and phase factors. Both of these conditions are satisfied by a long homogeneous circular cylinder with illumination incident perpendicularly to its axis.

APPENDIX A

Properties of the modulus and phase factors of Riccati-Bessel functions are as follows.

1. Definitions

The Riccati-Bessel functions are related to spherical Bessel functions $j_n(z)$ and $n_n(z)$ by

$$\psi_n(z)=zj_n(z), \quad \chi_n(z)=zn_n(z) \tag{A1}$$

and are expressible in the forms

$$\psi_n(z)=M_n(z)\sin\vartheta_n(z), \quad \chi_n(z)=-M_n(z)\cos\vartheta_n(z), \tag{A2}$$

$$\psi_n'(z)=N_n(z)\cos\phi_n(z), \quad \chi_n'(z)=N_n(z)\sin\phi_n(z), \tag{A3}$$

in which the primes denote differentiation with respect to z. These definitions match our requirements $\psi_0(z)=\sin z$ and $\chi_0(z)=-\cos z$, while for large orders $\psi_n(z)\to 0$ and $\psi_n'(z)\to 0$ imply $\vartheta_n(z)\to 0$ and $\phi_n(z)\to\pi/2$ when $n\to\infty$. The moduli $M_n(z), N_n(z)$ and phase factors $\vartheta_n(z), \phi_n(z)$ may then be obtained from

$$M_n^2(z)=\psi_n^2(z)+\chi_n^2(z), \quad N_n^2(z)=\psi_n'^2(z)+\chi_n'^2(z), \tag{A4}$$

$$\vartheta_n(z)=\tan^{-1}\left\{-\frac{\psi_n(z)}{\chi_n(z)}\right\}, \quad \phi_n(z)=\tan^{-1}\left\{\frac{\chi_n'(z)}{\psi_n'(z)}\right\}. \tag{A5}$$

2. The Wronskian function

The Wronskian function

$$\psi_n(z)\chi_n'(z)-\psi_n'(z)\chi_n(z)=1 \tag{A6}$$

or by substitution

$$M_n(z)N_n(z)\cos\Delta_n(z)=1, \tag{A7}$$

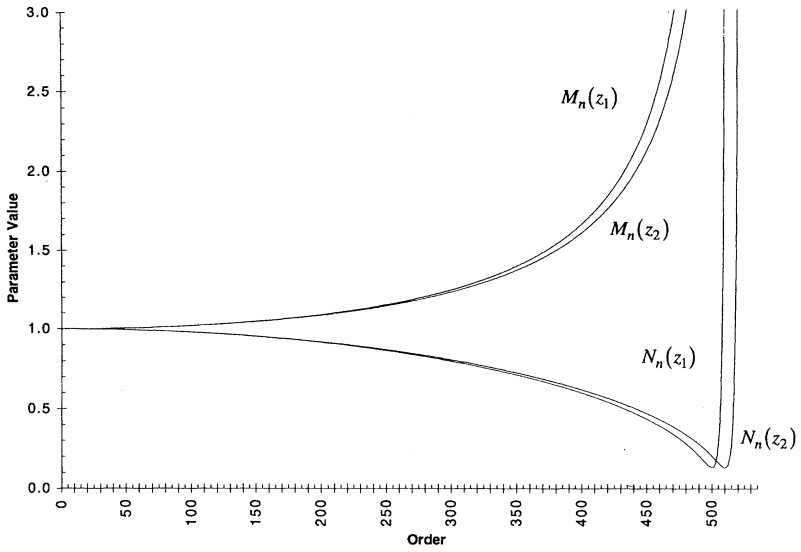

FIG. 16. Variation of $M_n(z)$ and $N_n(z)$ with order for $z_1=500.0$ and $z_2=510.5$.

where $\Delta_n(z)=\phi_n(z)-\vartheta_n(z)$.

3. Relations

Differentiation of Eqs. (A2) and the applications of Eqs. (A3) yields

$$N_n(z)\cos\Delta_n(z)=M_n(z)\vartheta_n'(z), \tag{A8}$$

$$N_n(z)\sin\Delta_n(z)=-M_n'(z). \tag{A9}$$

These may be converted into

$$M_n^2(z)\vartheta_n'(z)=1, \tag{A10}$$

$$\tan\Delta_n(z)=-M_n(z)M_n'(z)=-[\psi_n(z)\psi_n'(z)+\chi_n(z)\chi_n'(z)] \tag{A11}$$

by Eq. (A7). From Eqs. (A3) and (A7) we may also obtain

$$\psi_n'(z)=\frac{\cos[\vartheta_n(z)+\Delta_n(z)]}{M_n(z)\cos\Delta_n(z)},\quad \chi_n'(z)=\frac{\sin[\vartheta_n(z)+\Delta_n(z)]}{M_n(z)\cos\Delta_n(z)}. \tag{A12}$$

4. Expressions

$$M_n^2(z)=1+\frac{1}{2}\frac{\mu_1}{z^2}+\frac{1\times3}{2\times4}\frac{\mu_1\mu_2}{z^4}+\frac{1\times3\times5}{2\times4\times6}\frac{\mu_1\mu_2\mu_3}{z^6}+\cdots, \tag{A13}$$

$$\vartheta_n(z)=z-n\frac{\pi}{2}+\frac{\mu_1}{2z}+\frac{\mu_1(\mu_1-6)}{24z^3}+\frac{\mu_1(\mu_1^2-28\mu_1+60)}{80z^5}+\frac{\mu_1(5\mu_1^3-380\mu_1^2+3228\mu_1-5040)}{896z^7}+\cdots, \tag{A14}$$

$$\tan\Delta_n(z)=\frac{\mu_1}{2z^3}\left\{1+\frac{3}{2}\frac{\mu_2}{z^2}+\frac{3\times5}{2\times4}\frac{\mu_2\mu_3}{z^4}+\frac{3\times5\times7}{2\times4\times6}\frac{\mu_2\mu_3\mu_4}{z^6}+\cdots\right., \tag{A15}$$

in which $\mu_p=(n+p)(n-p+1)$. The series (A13) and (A15) terminate at $p=n$ and are exact, but the series (A14) only applies when n/z is small. Plots of the moduli and phase factors are presented in Figs. 16 and 17.

5. Approximations

When $n<z$,

$$M_n^2(z)=\frac{1}{\sqrt{1-(\mu_1/z^2)}}+O(n^2/z^4), \tag{A16}$$

$$\vartheta_n(z)=\sqrt{z^2-\mu_1}-n\tan^{-1}\left(\frac{\sqrt{z^2-\mu_1}}{n+1}\right)+O(n^3/z^3), \tag{A17}$$

$$\tan\Delta_n(z)=\frac{1}{2}\frac{\mu_1}{[z^2-\mu_1]^{3/2}}+O(n^2/z^5). \tag{A18}$$

But for $n+\frac{1}{2}=z$,

$$M_n^2(z)\approx1.257(z)^{1/3}, \tag{A19}$$

$$\vartheta_n(z)\approx\pi/6, \tag{A20}$$

$$\tan\Delta_n(z)\approx1/\sqrt{3}. \tag{A21}$$

APPENDIX B

The general solution of the multipole phase angles is as follows. The multipole phase angles are defined by

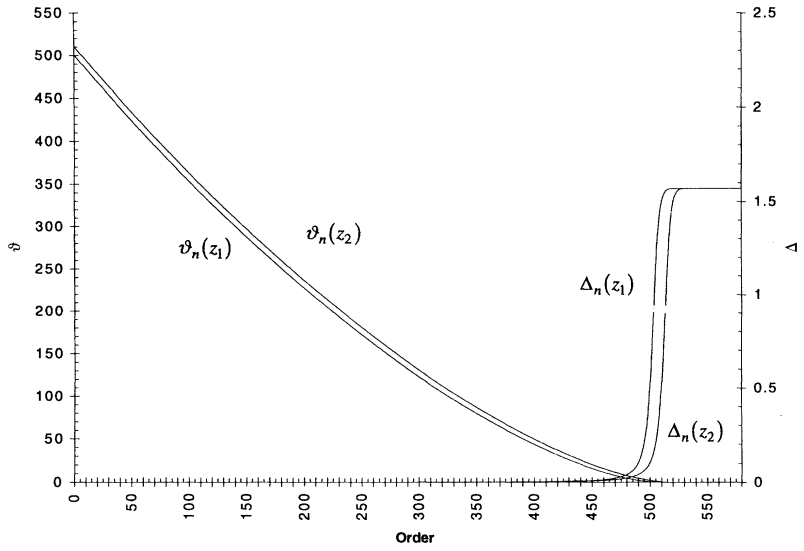

FIG. 17. Variation of $\vartheta_n(z)$ and $\Delta_n(z)$ with order for $z_1=500.5$ and $z_2=510.5$.

$$\tan u_n=\frac{\psi_n'(\beta)\psi_n(\alpha)-m\psi_n(\beta)\psi_n'(\alpha)}{\psi_n'(\beta)\chi_n(\alpha)-m\psi_n(\beta)\chi_n'(\alpha)}, \tag{B1a}$$

$$\tan v_n=\frac{m\psi_n'(\beta)\psi_n(\alpha)-\psi_n(\beta)\psi_n'(\alpha)}{m\psi_n'(\beta)\chi_n(\alpha)-\psi_n(\beta)\chi_n'(\alpha)}. \tag{B1b}$$

Substitution of expressions (A2) and (A12) into the above equations then results in

$$\tan\begin{Bmatrix}u_n\\v_n\end{Bmatrix}=\frac{a\ \tan\vartheta_n(\beta)-b\ \tan\vartheta_n(\alpha)-c\ \tan\vartheta_n(\alpha)\tan\vartheta_n(\beta)}{c\ \tan\vartheta_n(\beta)+a\ \tan\vartheta_n(\alpha)\tan\vartheta_n(\beta)+b}, \tag{B2}$$

where for

$$u_n:\quad a=m/M_n^2(\alpha),\quad b=1/M_n^2(\beta);$$
$$v_n:\quad a=1/M_n^2(\alpha),\quad b=m/M_n^2(\beta);$$

and $c=a\ \tan\Delta_n(\alpha)-b\ \tan\Delta_n(\beta)$. It should be noted that a and b are always positive, but the sign of c is positive for $m>1$ and negative when $m<1$.

We wish to show that the phase angles can be written as

$$\tan\begin{Bmatrix}u_n\\v_n\end{Bmatrix}=\frac{\sigma\ \tan[\vartheta_n(\beta)+\tau]-\tan[\vartheta_n(\alpha)+\rho]}{1+\sigma\ \tan[\vartheta_n(\beta)+\tau]\tan[\vartheta_n(\alpha)+\rho]}. \tag{B3}$$

To this end, the tangent terms in Eq. (B3) are expanded and the resulting expression compared with Eq. (B2) gives

$$0=\sigma\ \tan\tau-\tan\rho, \tag{B4a}$$

$$\gamma a=\sigma+\tan\rho\ \tan\tau, \tag{B4b}$$

$$\gamma b=1+\sigma\ \tan\rho\ \tan\tau, \tag{B4c}$$

$$\gamma c=\sigma\ \tan\rho-\tan\tau, \tag{B4d}$$

in which γ is a common factor. These may be reduced by using Eq. (B4a) to

$$\gamma a=\sigma(1+\tan^2\tau), \tag{B5a}$$

$$\gamma b=1+\sigma^2\tan^2\tau, \tag{B5b}$$

$$\gamma c=(\sigma^2-1)\tan\tau. \tag{B5c}$$

Since a and b are always positive, so also are γ and σ by Eqs. (B5b) and (B5a), respectively. The sign of $\tan\tau$ given by Eq. (B5c) is more complex and leads to solutions that may be classified into two domains as shown in Fig. 18. γ may be eliminated from Eqs. (B5) by the combinations

$$\frac{a^2+b^2+c^2}{2ab}=\frac{1+\sigma^2}{2\sigma}, \tag{B6a}$$

$$\frac{a^2-b^2+c^2}{2bc}=\frac{1-\tan^2\tau}{2\tan\tau} \tag{B6b}$$

to give solutions

$$\sigma=e^{\pm\kappa}, \tag{B7}$$

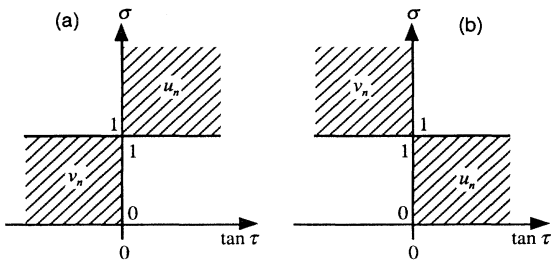

FIG. 18. Domains of the multipole phase angles for (a) $m>1$, $c>0$, and (b) $m<1$, $c<0$.

$$\tan\tau=\begin{cases} e^{-\lambda} \\ -e^{\lambda}, \end{cases} \tag{B8}$$

where

$$\cosh\kappa=\frac{a^2+b^2+c^2}{2ab}, \tag{B9}$$

$$\sinh\lambda=\frac{a^2-b^2+c^2}{2bc}. \tag{B10}$$

We note that κ may always be taken as positive, but λ may be either positive or negative. The particular choice of solution is obtained from Fig. 18 as follows. When $m>1$ and $c>0$,

$$u_n: \quad \sigma=e^{\kappa}, \quad \tan\tau=e^{-\lambda}; \tag{B11a}$$

$$v_n: \quad \sigma=e^{-\kappa}, \quad \tan\tau=-e^{\lambda}, \tag{B11b}$$

but for $m<1$ and $c<0$,

$$u_n: \quad \sigma=e^{-\kappa}, \quad \tan\tau=e^{-\lambda}; \tag{B12a}$$

$$v_n: \quad \sigma=e^{\kappa}, \quad \tan\tau=-e^{\lambda}. \tag{B12b}$$

As Eq. (B3) has now been verified, we may proceed with its inversion. Letting

$$\sigma\ \tan[\vartheta_n(\beta)+\tau]=\tan[\vartheta_n(\beta)+\tau+\epsilon_1], \tag{B13}$$

then

$$\tan\epsilon_1=\frac{(\sigma-1)\tan[\vartheta_n(\beta)+\tau]}{1+\sigma\ \tan^2[\vartheta_n(\beta)+\tau]}. \tag{B14}$$

Similarly,

$$\tan\rho=\sigma\ \tan\tau=\tan(\tau+\epsilon_2) \tag{B15}$$

gives

$$\rho=\tau+\epsilon_2, \tag{B16}$$

where

$$\tan\epsilon_2=\frac{(\sigma-1)\tan\tau}{1+\sigma\ \tan^2\tau}. \tag{B17}$$

Thus Eq. (B3) may be written as

$$\tan\begin{Bmatrix} u_n \\ v_n \end{Bmatrix}=\frac{\tan[\vartheta_n(\beta)+\tau+\epsilon_1]-\tan[\vartheta_n(\alpha)+\tau+\epsilon_2]}{1+\tan[\vartheta_n(\beta)+\tau+\epsilon_1]\tan[\vartheta_n(\alpha)+\tau+\epsilon_2]}, \tag{B18}$$

with the solution

$$\begin{Bmatrix} u_n \\ v_n \end{Bmatrix}=[\vartheta_n(\beta)+\tau+\epsilon_1]-[\vartheta_n(\alpha)+\tau+\epsilon_2]$$
$$=\vartheta_n(\beta)-\vartheta_n(\alpha)+\epsilon_1-\epsilon_2. \tag{B19}$$

Separation of the solution into dominant and incremental components then yields

$$\begin{Bmatrix} \tilde{u}_n \\ \tilde{v}_n \end{Bmatrix}=\vartheta_n(\beta)-\vartheta_n(\alpha) \tag{B20}$$

and

$$\begin{Bmatrix} \tilde{u}_n \\ \tilde{v}_n \end{Bmatrix}=\epsilon_1-\epsilon_2=\tan^{-1}\left\{\frac{(\sigma-1)\tan[\vartheta_n(\beta)+\tau]}{1+\sigma\ \tan^2[\vartheta_n(\beta)+\tau]}\right\}$$
$$-\tan^{-1}\left\{\frac{(\sigma-1)\tan\tau}{1+\sigma\ \tan^2\tau}\right\}. \tag{B21}$$

Both ϵ_1 and ϵ_2 lie in the range $-\pi/2$ to $+\pi/2$.

[1] Z. J. Ulanowski, I. K. Ludlow, and W. M. Waites, FEMS Microbiol. Lett. **40**, 229 (1987).

[2] Z. J. Ulanowski and I. K. Ludlow, Mycolog. Res. **93**, 28 (1989).

[3] L. A. de Pieri, I. K. Ludlow, and W. M. Waites, J. Appl. Bacteriol. **74**, 578 (1993).

[4] I. K. Ludlow and J. Everitt, Phys. Rev. E **51**, 2516 (1994).

[5] M. Kerker, *The Scattering of Light and Other Electromagnetic Radiation* (Academic, New York, 1969).

[6] Handbook of Mathematical Functions, Natl. Bur. Stand. Appl. Math. Ser. No. 55, edited by M. Abramowitz and I. A. Stegun (U.S. GPO, Washington, 1964).